A self-blinking DNA probe for 3D superresolution imaging of native chromatin

Yang Zheng[1,2,10], Sen Ye[1,10], Shumin Li[3,10], Cuifang Liu[4,5], Shihang Luo[5,6], Ruiqin Xia[1], Yanqin Chen[2], Yunsheng Li[2], Zhenni Zhu[7], Lingyi Huang[2], Shan Deng[1], Karen Wing Yee Yuen[7], Ping Chen[4,8], Yongdeng Zhang[2], Wei Ji[5,6], Ruibang Luo[3], Guohong Li[4,5,9]* & Dan Yang[1,2]*

[1]Morningside Laboratory for Chemical Biology and Department of Chemistry, The University of Hong Kong, Hong Kong, China.

[2]School of Life Sciences, Westlake University, Hangzhou, Zhejiang, China.

[3]Department of Computer Science, The University of Hong Kong, Hong Kong, China.

[4]National Laboratory of Biomacromolecules, CAS Center for Excellence in Biomacromolecules, Institute of Biophysics, Chinese Academy of Sciences, Beijing, China.

[5]College of Life Science, University of Chinese Academy of Sciences, Beijing, China.

[6]Institute of Biophysics, Chinese Academy of Sciences, Beijing, China.

[7]School of Biological Sciences, The University of Hong Kong, Hong Kong, China.

[8]Department of Immunology, School of Basic Medical Sciences, Advanced Innovation Center for Human Brain Protection, Capital Medical University, Beijing, China.

[9]Bioland Laboratory (Guangzhou Regenerative Medicine and Health Guangdong Laboratory), Guangzhou, Guangdong, China.

[10]These authors contributed equally: Yang Zheng, Sen Ye, Shumin Li.

*Correspondence: Guohong Li (liguohong@ibp.ac.cn) or Dan Yang (yangdan@westlake.edu.cn).

ABSTRACT

Single-molecule localization microscopy is a powerful superresolution imaging technique to study biological questions by visualizing subcellular fine structures with nanometer-scale precision. However, its application in live-cell imaging studies has been impeded by the paucity of self-blinking organic

fluorophores that enable high spatiotemporal resolution and labeling/localization density at a moderate laser intensity. Herein, we report a self-blinking Si-rhodamine dye **6-HESiR** with a suitably increased "ON" fraction and a fluorogenic self-blinking dsDNA probe **6-HoeHESiR** as a powerful tool for 3D superresolution imaging of native chromatin in eukaryotes without the use of photoswitching buffer and high laser intensity. With the probe **6-HoeHESiR**, 3D superresolution imaging of in vitro reconstituted nucleosomal arrays and chromatin fibers yielded results consistent with EM analysis. Similar euchromatin and heterochromatin structures were visualized in fixed and live cells with high spatiotemporal resolution and labeling density, providing the first live-cell evidence for a hierarchical model of chromatin organization. 3D imaging results obtained in the presence of selective inhibitors of histone deacetylases also corroborate chromatin fiber decompaction upon hyperacetylation of histones.

INTRODUCTION

Superresolution fluorescence microscopy is a powerful tool for interrogating important biological questions. By bypassing the diffraction limit of light, superresolution microscopy has been developed to visualize previously unresolvable fine subcellular structures with nanometer-scale precision[1-6]. However, the best-performing commercial organic dyes (e.g., Alexa 647) widely used for single-molecule localization microscopy (SMLM) still suffer from poor cell permeability and the need for photoswitching buffers that are highly reducing and incompatible with live cells[2,6]. Such limitations have impeded the study of important biological questions by live-cell SMLM. In recent years, self-blinking organic fluorophores such as **HMSiR**[7-10] were developed for SMLM of living cells without using live-cell incompatible photoswitching buffers and 405-nm laser. Yet, high-quality imaging results with high spatiotemporal resolution and labeling density were only achieved in 2D imaging of endoplasmic reticulum (ER)[11] with very high laser intensity[12]. It is still a formidable challenge to achieve high spatiotemporal resolution and labeling density in 3D live-cell SMLM, even at a moderate excitation laser intensity. In principle, the number of "ON" state fluorophores in each frame should be

as high as possible to minimize the acquisition time, yet low enough to avoid PSF overlaps[6]. In this work, we have developed a self-blinking Si-rhodamine dye **6-HESiR** with a suitably increased "ON" fraction by employing the structural fine-tuning strategy[13-15]. By connecting **6-HESiR** to a Hoechst fragment for DNA minor groove binding, we have obtained a self-blinking fluorogenic probe **6-HoeHESiR** for imaging native chromatin in living cells. This probe has been validated with lambda DNA, *in vitro* reconstituted nucleosomal arrays and 30-nm chromatin fibers, and our 3D imaging results are consistent with those obtained by EM analysis. The 3D visualization of both nucleosomal arrays and chromatin fibers in fixed cells and living cells has been achieved with high spatiotemporal resolution and labeling density at low laser intensity to minimize phototoxicity. We have observed structural plasticity of chromatin fibers in both HeLa cells and chicken erythrocytes. Fast chromatin fiber dynamics were captured with less than 2-second temporal resolution, and the mean resting/dwelling lifetime of chromatin fibers was estimated to be 0.6 seconds in HeLa cells and 1 second in chicken erythrocytes. We have also observed the decompaction of chromatin fibers induced by small-molecule inhibitors of histone deacetylases (HDACs), providing the first live-cell evidence for the direct link between histone acetylation state and 3D chromatin organization with unprecedented resolution.

RESULTS

The development of a self-blinking fluorogenic DNA probe

To achieve high spatiotemporal resolution and labeling density in 3D live-cell SMLM, we conceived a design strategy for self-blinking fluorophores with the following criteria: 1) absorption maximum in the deep red and near infrared regions to minimize autofluorescence and phototoxicity to living cells[12]; 2) a fine-tuned fluorescent "ON" state population for optimal localization number per frame to achieve sufficient labeling density in a short acquisition time while preventing PSF overlap[6]; 3) take into account the pH and hydrophobicity that influence the "ON" state population[11]. To meet the above criteria, we developed a self-blinking Si-rhodamine dye **6-HESiR** (Fig. 1a-b) by replacing the hydroxymethyl group of **HMSiR**[7] with a hydroxyethyl group[16,17]. This type of self-blinking dyes is

75 expected to undergo equilibrium between the open form (fluorescent "ON" state) and the closed form
76 ("OFF" state) with an equilibrium constant as K_{cycl}. For entropic reason, formation of the
77 six-membered-ring cyclic form ('OFF" form) for **6-HESiR** should be more difficult than that of the
78 five-membered-ring cyclic form of **HMSiR**. As a result, **6-HESiR** should favor the open form more
79 than **HMSiR**, and hence increasing the localization number per frame significantly for fast acquisition
80 of sufficient localizations to resolve dynamic fine structures. This new fluorophore **6-HESiR** was
81 successfully prepared through an efficient synthetic route (shown in Supplementary Information), and
82 the "ON" state population of **6-HESiR** was estimated from the absorption spectra to be 20% at
83 physiological pH (7.4) in aqueous buffer with **SiR650** as the benchmark of the 100% "ON" state (Fig.
84 1b-c, Supplementary Fig. 1). In addition, based on the pH titration curve (Fig. 1d), we determined the
85 pK_{cycl} value of **6-HESiR** to be 6.6, higher than that of **HMSiR** (pK_{cycl} = 5.8, Fig. 1a).
86 The successful implementation of live-cell SMLM hinges not only on the self-blinking fluorophore but
87 also on a fully biocompatible labeling strategy that is noninvasive, highly selective, and artifact-free
88 with high labeling density. In this regard, we chose the Hoechst tagging strategy[18], as it has found some
89 success in developing fluorogenic probes for live-cell chromatin imaging[18-23] with low cytotoxicity. The
90 Hoechst moiety could noncovalently bind to the DNA minor groove in a highly selective manner.
91 Therefore, we designed and synthesized **6-HoeHESiR** by connecting **6-HESiR** and the Hoechst
92 fragment with a carbamate linker (Fig. 1e). The *in vitro* binding of **6-HoeHESiR** to a benchmark hairpin
93 DNA (hpDNA) molecule (Fig. 1f) with an AATT Hoechst binding site[24] was examined by fluorescence
94 titration. In the absence of hpDNA, the fluorescence of **6-HoeHESiR** was nearly quenched (Fig. 1h). A
95 dose-dependent fluorescence turn-on was observed upon the addition of increasing equivalents of
96 hpDNA to **6-HoeHESiR** (Fig. 1g). A 43-fold fluorescence increase (Fig. 1h) with 14 μM of hpDNA
97 confirmed the sensitivity and fluorogenicity of **6-HoeHESiR**. Based on the titration curve (Fig. 1g), the
98 dissociation constant (K_D) of the complex formed by **6-HoeHESiR** and hpDNA was estimated to be 3.8
99 μM. The attachment of **6-HESiR** to the Hoechst dye caused a slight redshift of both the absorbance and

fluorescence maxima of **6-HoeHESiR** (Supplementary Fig. 2a-b). Upon the addition of hpDNA (14 μM), the absorbance of **6-HoeHESiR** was increased to a level close to that of the free fluorophore **6-HESiR** (Supplementary Fig. 2a), and the fluorescence of **6-HoeHESiR** was recovered to 21% of that of **6-HESiR** (Supplementary Fig. 2b).

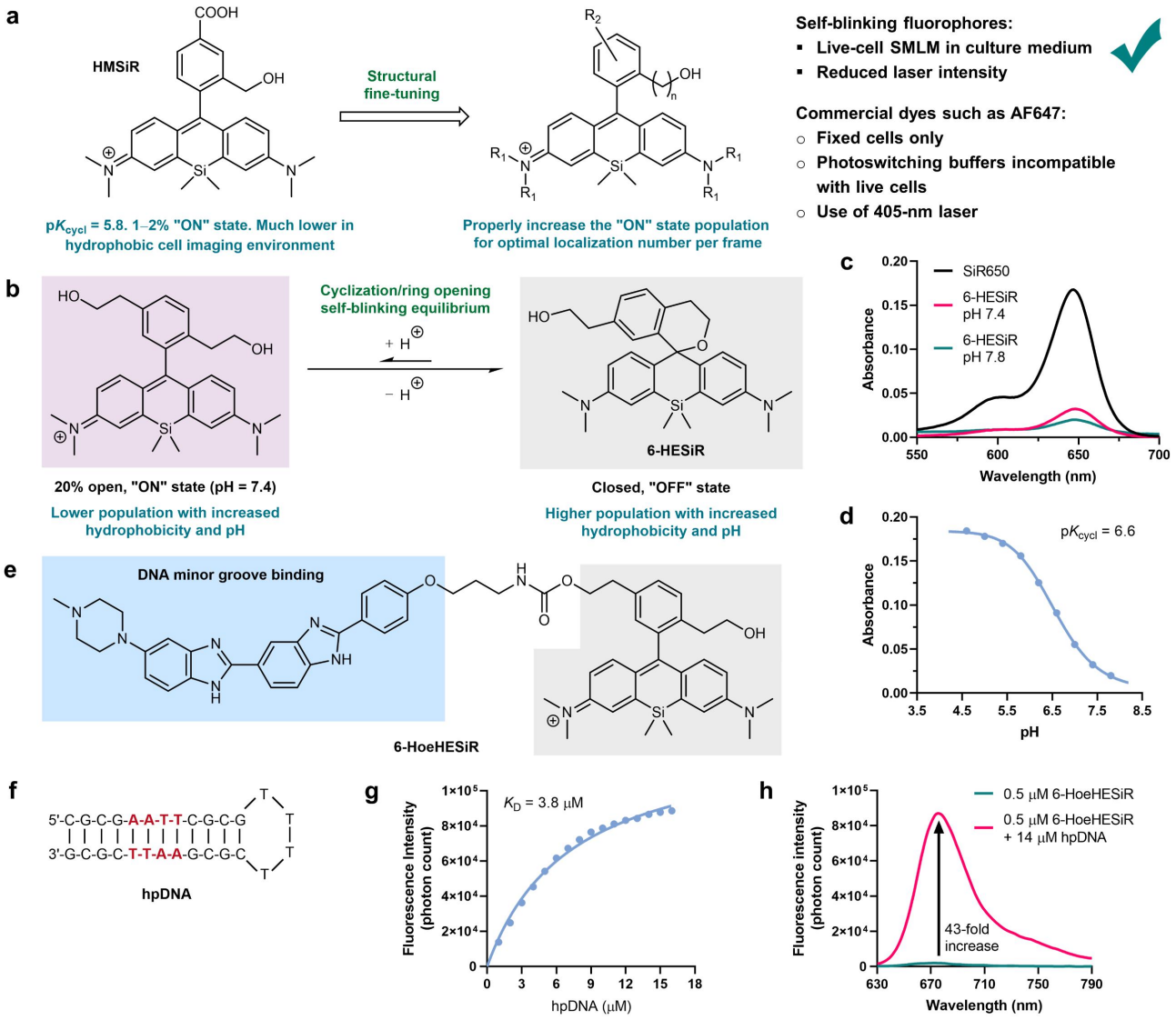

Fig. 1 Development of 6-HESiR and 6-HoeHESiR. a, Structural fine-tuning strategy for developing self-blinking fluorophores. **b**, Self-blinking mechanism. **c**, Absorption spectrum of **6-HESiR** (2 μM) in 0.1 M potassium phosphate buffer (pH = 7.4 and 7.8) with **SiR650** (2 μM) as the "100%" benchmark. Abs_{max} at 648 nm. Fl_{max} at 665 nm. **d**, pH titration of **6-HESiR** (2 μM) in 0.1 M potassium phosphate buffer. **e**, Design of **6-HoeHESiR** by Hoechst tagging strategy. **f**, The hpDNA for fluorescence titration.

110 **g**, Fluorescence titration of **6-HoeHESiR** (0.5 μM) with hpDNA (0−16 μM) in Tris-HCl saline buffer
111 (50 mM Tris-HCl, 100 mM NaCl, pH = 7.4). Fl_{max} at 676 nm. **h**, Fluorescence increases 43-fold in the
112 presence of 14 μM hpDNA.

113 **Validation with lambda DNA and *in vitro* reconstituted chromatin structures**

114 To evaluate our new probe **6-HoeHESiR**, we first attempted an SMLM experiment of spin-coated
115 lambda DNA[25] with $(A/T)_4$ binding sites for the Hoechst moiety[24]. A full width at half maximum
116 (FWHM) of 26 nm was successfully obtained (Supplementary Fig. 3), which is within the range of
117 20–30 nm as reported in literature[25]. Then, we focused on *in vitro* reconstituted nucleosomal arrays and
118 30-nm chromatin fibers as benchmarks previously well characterized by EM[26] (Fig. 2d and 2f,
119 Supplementary Fig. 4a and 4e). Apart from the AATT binding site, three additional Hoechst binding
120 sites[24] in the DNA template for *in vitro* reconstituted chromatin samples were also identified by
121 fluorescence titration (Fig. 2a, Supplementary Fig. 2c-f). Based on the dissociation constants, the
122 half-life of the complex formed by **6-HoeHESiR** and a nucleosome was estimated to be 10–20 ms[24].
123 Thus, fast binding/dissociation cycles between **6-HoeHESiR** and nucleosomes could allow fast
124 self-blinking with a pool of **6-HoeHESiR** molecules in the unbound state (Fig. 2b). Since the
125 hydrophobic environment in the nucleus favors the closed "OFF" state[11] (Fig. 1b) and the open form of
126 **6-HoeHESiR** in the unbound state is nearly quenched in fluorescence (Fig. 1h), the "ON" state
127 population of **6-HoeHESiR** in chromatin imaging is expected to be lower than the 20% "ON" fraction
128 of **6-HESiR** measured in aqueous buffer. Gratifyingly, **6-HoeHESiR** exhibited excellent self-blinking
129 in SMLM experiments on reconstituted chromatin samples at a modest laser intensity[12] of 950 W/cm^2
130 (Supplementary Video 1). The reconstituted nucleosomal arrays displayed the pattern of discrete
131 fluorescence signals (Fig. 2c and 2e, Supplementary Fig. 4b), which resembles the EM images (Fig. 2d,
132 Supplementary Fig. 4a). Analysis of localizations on individual nucleosomes indicated that the ratio of
133 axial to lateral resolution is 2.3 (Supplementary Fig. 4c-d). To extract 3D structural features of
134 reconstituted 30-nm chromatin fibers visualized in 3D SMLM experiments (Fig. 2c and 2g;

135 Supplementary Fig. 4f), we developed an image analysis program (Supplementary Fig.5 and 6,
136 Supplementary Information). Statistical results showed that the reconstituted chromatin fibers had a
137 mean diameter of 32 nm, length of 108 nm, mean localization precision of 7.8 nm and labeling density
138 of 31,815 molecules/μm^3 (Fig. 2h, Supplementary Fig. 4g, Supplementary Video 2 and 3). Although the
139 reconstituted 30-nm fibers without biotin labels were visualized by EM in a dry and flattened state
140 (Supplementary Information), unlike our 3D SMLM approach, the 3D structural features obtained with
141 **6-HoeHESiR** were consistent with those revealed by EM (Fig. 2f-h). Some elongated fibers were
142 observed, probably due to slight loosening in the aqueous buffer without chemical crosslinker compared
143 with the dry and crosslinked state in EM analysis.

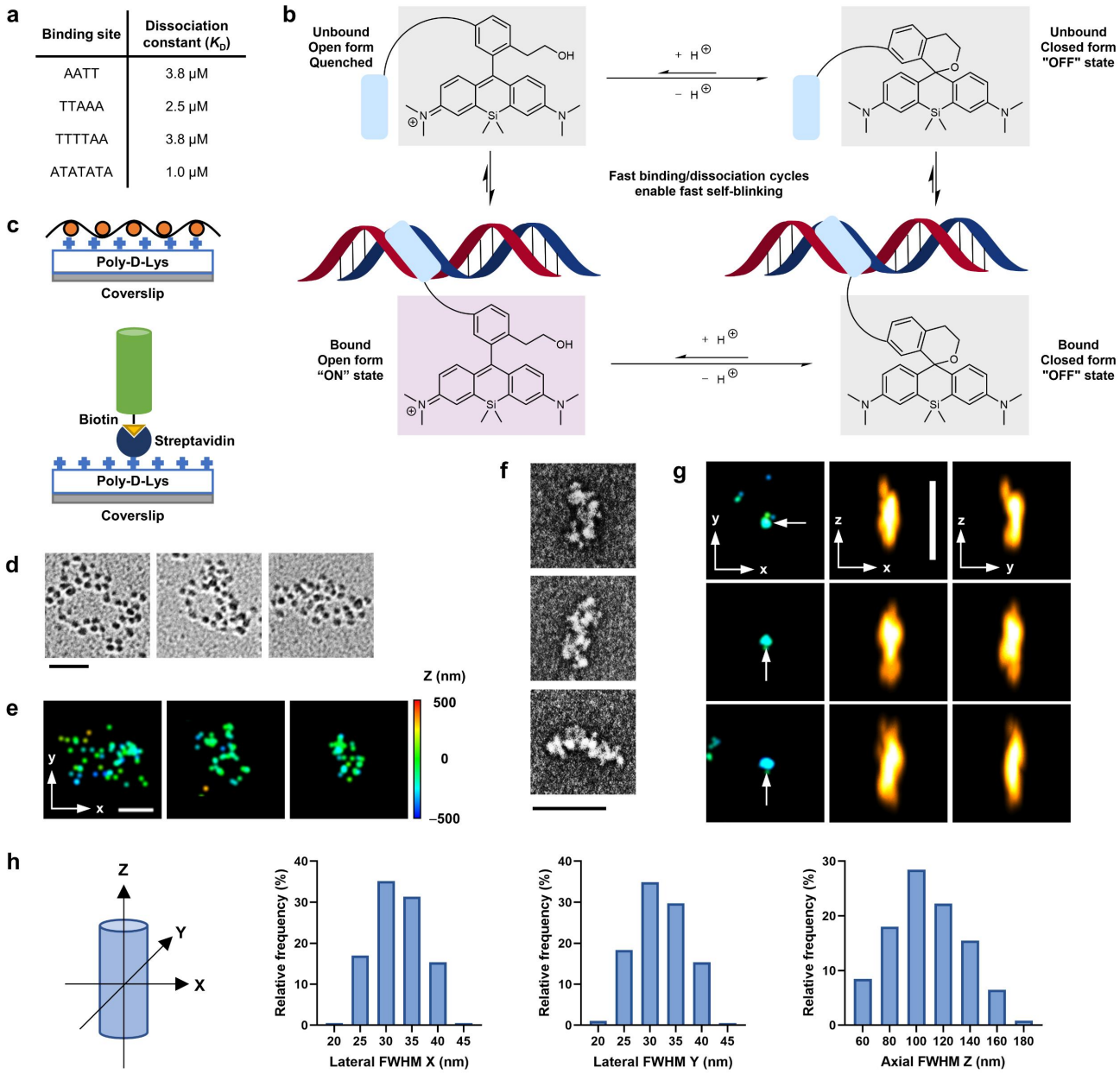

Fig. 2 in vitro reconstituted chromatin structures. a, Dissociation constants of four binding sites in the DNA template. **b**, Working mechanism of **6-HoeHESiR** in the presence of nucleosomes. **c**, Immobilization approaches for 40 × 187-bp nucleosomal arrays and 30-nm chromatin fibers. **d**, EM images of nucleosomal arrays. **e**, Images of nucleosomal arrays by 3D SMLM. **f**, EM images of 30-nm chromatin fibers. **g**, Images of 30-nm chromatin fibers by 3D SMLM. 3D sizes by FWHM (x, y, z) in nm (from top to bottom): 29, 30, 93; 30, 30, 101; 34, 26, 104. Localization precision (nm): 5.5, 5.9, 6. **h**, Histograms of 3D sizes of chromatin fibers. N = 370 from 3 fields of view. Incubation with

152 **6-HoeHESiR** (2.5 μM) for 10 min. Scale bar: 100 nm in **d** and **f**; 200 nm in **e** and **g**. Laser intensity:
153 0.95 kW/cm^2 at 656 nm. Axial position (nm) represented by RGB color depth coding.

154 **Native chromatin 3D structures in fixed cells**

155 Building upon the solid validation of **6-HoeHESiR** in SMLM of *in vitro* reconstituted nucleosomal
156 arrays and 30-nm chromatin fibers, we then attempted to image native chromatin structures in fixed
157 HeLa cells (Fig. 3a, Supplementary Fig. 7a, Supplementary Video 4). Based on the structural
158 resemblance to *in vitro* reconstituted benchmark chromatin samples, we identified two categories of
159 chromatin structures. The first category consists of nucleosomal arrays (Fig. 3b), which displayed the
160 same pattern of discrete fluorescence signals (Fig. 2d). The second category consists of chromatin fibers
161 with structural plasticity (Fig. 3c, Supplementary Fig. 7b). With the aid of the image analysis program,
162 these fibers were identified with a mean localization precision of 8 nm, average 3D size (FWHM) of 30,
163 31, 101 nm (x, y, z) and a labeling density of 42,170 molecules/μm^3 (Fig. 3d, Supplementary Fig. 7d,
164 Supplementary Video 5 and 6). The overlay of widefield images showed that the chromatin fibers reside
165 in both the peripheral and the interior regions of the nuclei (Fig. 3e; Supplementary Fig. 7c). Budding
166 yeast *Saccharomyces cerevisiae* is a unicellular model organism for biological study. Yet, there has
167 been no 3D superresolution imaging of budding yeast chromatin. Therefore, we cultured *S. cerevisiae*
168 BY4741 cells and visualized their native chromatin with **6-HoeHESiR** after fixation (Fig. 3f-g,
169 Supplementary Fig. 8a, Supplementary Video 7). We were able to identify nucleosomal arrays and
170 chromatin fibers as the two categories of chromatin structures (Fig. 3h, 3i and 3k, Supplementary Fig.
171 8b and 8c). Chromatin fibers were visualized with a mean localization precision of 8.4 nm, average 3D
172 size (FWHM) of 34, 34, 113 nm (x, y, z) and a labeling density of 35,403 molecules/μm^3 (Fig. 3j,
173 Supplementary Fig. 8d, Supplementary Video 8 and 9). Our imaging results provide direct evidence that
174 agrees with recent studies by RICC-seq[27] and Micro-C genomics[28] that support the existence of
175 chromatin fibers in mammalian cells and budding yeasts.

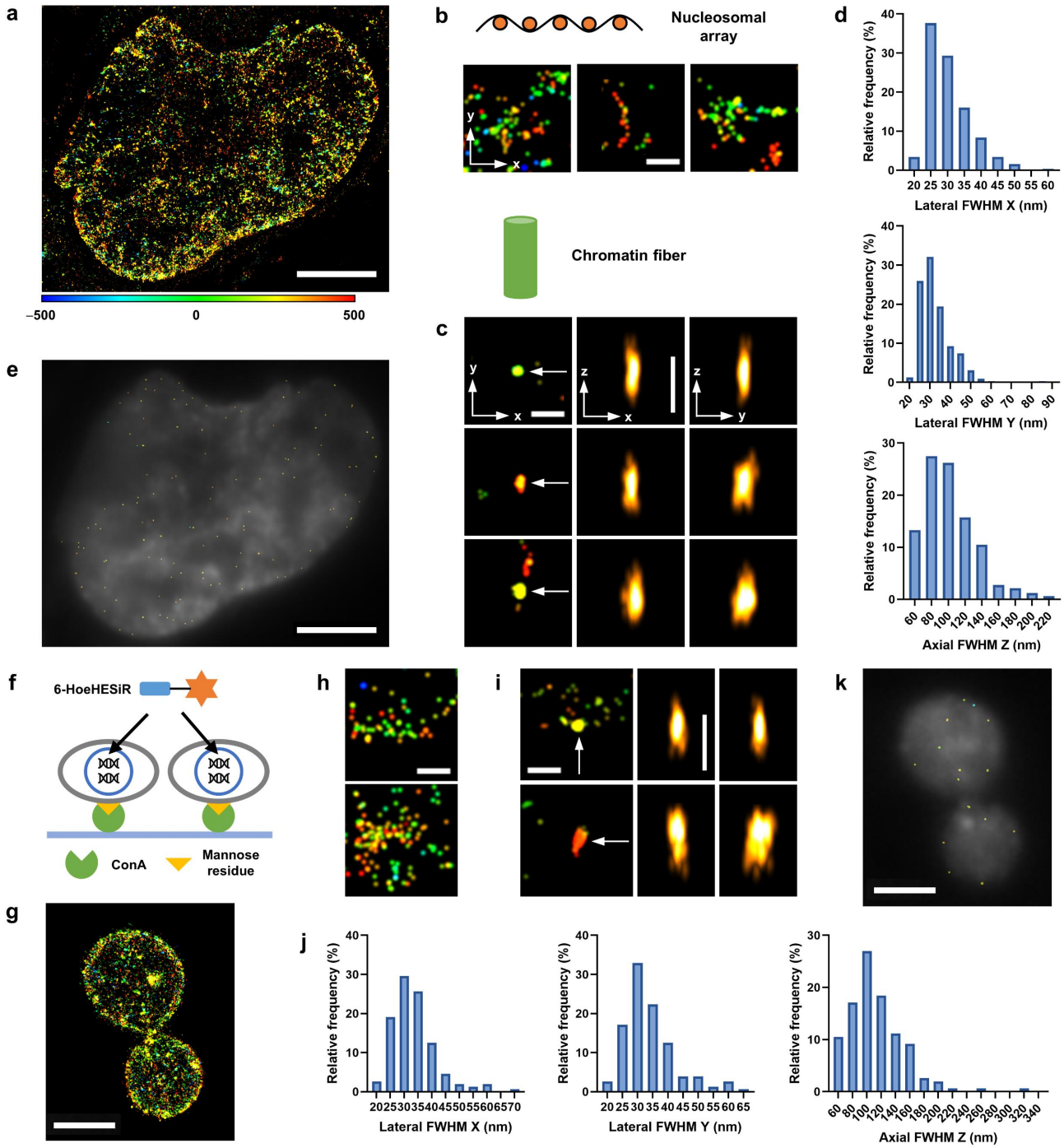

Fig. 3 Native chromatin 3D structures in fixed cells. a, Image of the nucleus in a HeLa cell. Reconstructed from 5,000 frames (17.7 ms/frame). **b,** Nucleosomal arrays in HeLa cells. **c,** Chromatin fibers in HeLa cells. FWHM (x, y, z) in nm (from top to bottom): 30, 27, 104; 26, 41, 108; 36, 51, 87. Localization precision (nm): 6.9, 6.1, 9.1. **d**, 3D sizes of chromatin fibers by FWHM. N = 324 from 3 HeLa cells, identified in 500 frames. **e**, Distribution of chromatin fibers in a HeLa cell. **f,**

182 Immobilization approach for imaging budding yeasts. **g,** The nuclei of two dividing budding yeasts. **h,**
183 Nucleosomal arrays in budding yeasts. **i,** Chromatin fibers in budding yeasts. FWHM (x, y, z) in nm
184 (from upper to lower): 32, 27, 94; 36, 62, 118. Localization precision (nm): 7, 9.2. **d**, 3D sizes of
185 chromatin fibers by FWHM. N = 152 from 16 budding yeast cells, identified in 500 frames. **k**,
186 Distribution of chromatin fibers in budding yeasts. Scale bar: 5 μm in **a** and **e**; 2 μm in **g** and **k**; 200 nm
187 in **b**, **c**, **h** and **i**. Laser intensity: 3.2 kW/cm^2 at 656 nm. Axial position (nm) represented by RGB color
188 depth coding.

189 **Native chromatin 3D structures in living cells**

190 First, we optimized the incubation conditions of **6-HoeHESiR** with living HeLa cells by light-sheet
191 microscopy (Fig. 4a-b, Supplementary Fig. 9a-b). To our delight, **6-HoeHESiR** exhibited good cell
192 permeability and high selectivity to provide 3D visualization of chromatin structures in whole nuclei.
193 Without the Hoechst fragment, **6-HESiR** did not stain any nuclear component (Supplementary Fig. 9c).
194 The cytotoxicity assay showed that **6-HoeHESiR** caused negligible toxicity with a short incubation time
195 (Supplementary Fig. 9d). Subsequent 3D SMLM experiments showed that **6-HoeHESiR** maintained its
196 excellent self-blinking capacity in living HeLa cells (Supplementary Video 10), and native chromatin
197 structures were clearly revealed (Fig. 4c; Supplementary Fig. 10a). We identified two categories of
198 chromatin structures in living HeLa cells, namely, nucleosomal arrays and chromatin fibers (Fig. 4d, 4e
199 and 4g, Supplementary Fig. 10b and 10d). Using the image analysis program, these fibers were
200 identified with a mean localization precision of 7.4 nm, average 3D size (FWHM) of 36, 39, 103 nm (x,
201 y, z) and a labeling density of 32,149 molecules/μm^3 (Fig. 4f, Supplementary Fig. 10c, Supplementary
202 Videos 11 and 12). The statistical distribution of 3D sizes and long-to-short fiber diameter ratios and the
203 heterogeneity of visualized morphologies reflect the structural polymorphism of chromatin fibers. Our
204 2D imaging results are consistent with recent reports[29,30,23] that nucleosome clutches or chromatin
205 domains were observed with no clear evidence of horizontally or randomly oriented chromatin fibers.
206 However, our 3D analysis, performed both manually and by the computer analysis program, identified

207 chromatin fibers oriented axially. We propose that such an ordered chromatin fiber orientation might not
208 only be consistent with highly regulated replication and transcription processes but facilitate these
209 processes. Remarkably, native chromatin structures in the nucleus are quite dynamic (Supplementary
210 Video 13). We captured transient chromatin fibers with a temporal resolution of less than 2 seconds (Fig.
211 4h; Supplementary Video 14). The mean resting/residing lifetime of chromatin fibers was estimated to
212 be 0.6 seconds (Supplementary Fig. 10c). This dwelling lifetime is comparable to the time scale of
213 folding and unfolding dynamics of *in vitro*-reconstituted 30-nm chromatin fibers revealed by
214 single-molecule force spectroscopy[26]. When the laser intensity was reduced to a modest level of 950
215 W/cm^2 from 3.2 kW/cm^2 to alleviate phototoxicity, nucleosomal arrays were visualized again, and we
216 could still identify chromatin fibers at sufficient resolution with a mean localization precision of 8.8 nm,
217 average 3D size (FWHM) of 35, 39, 108 nm (x, y, z) and a labeling density of 29,691 molecules/μm^3
218 (Supplementary Fig. 11). Fast chromatin dynamics were observed (Supplementary Video 15), and the
219 mean resting lifetime of chromatin fibers was estimated to be 0.6 seconds, consistent with the result
220 obtained at 3.2 kW/cm^2 laser intensity.

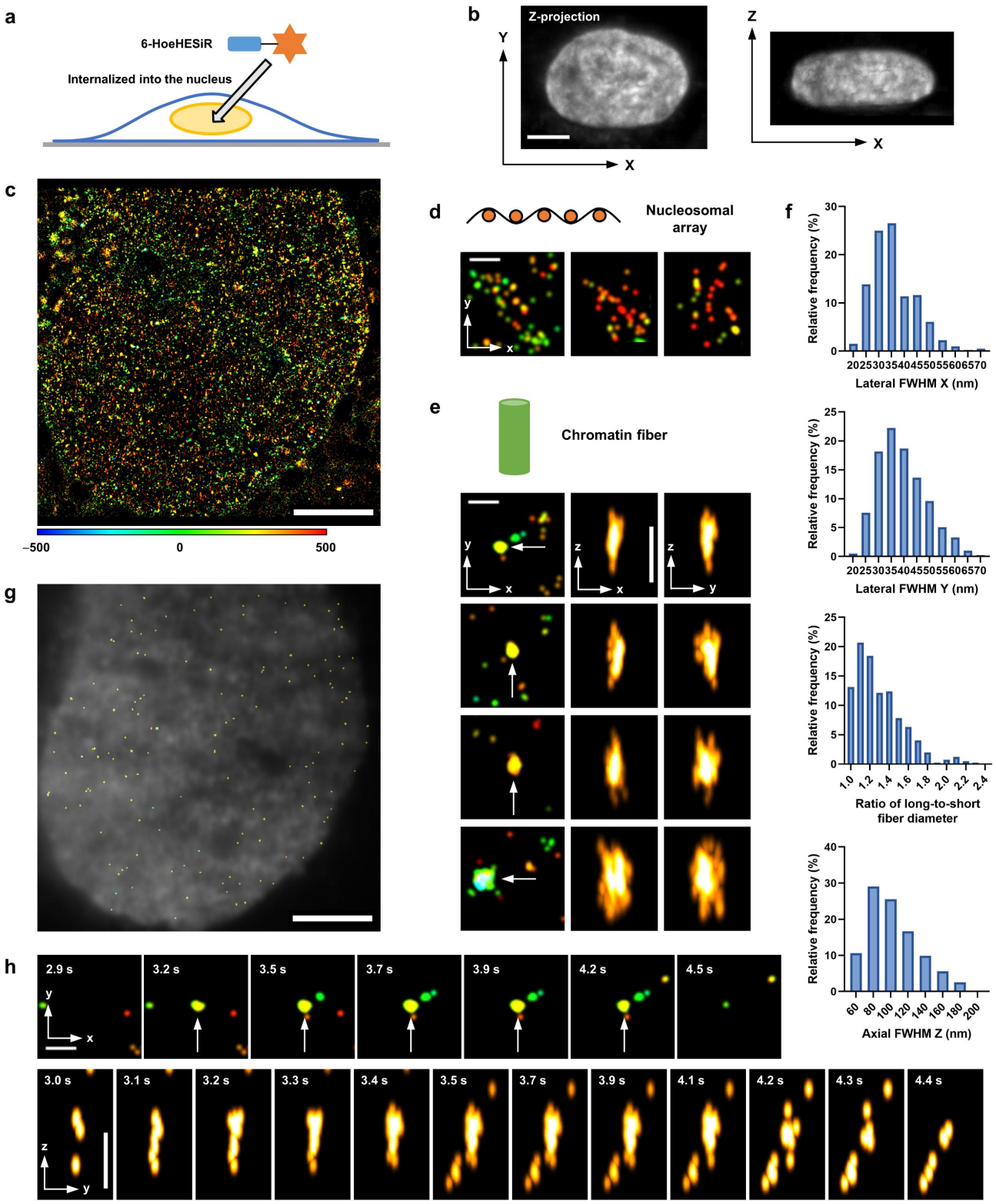

Fig. 4 Native chromatin 3D structures in living HeLa cells. a, Schematic illustration of chromatin labeling with **6-HoeHESiR** (5 μM for 30 min). **b,** Images of a whole nucleus by light-sheet microscopy. **c**, Image of a nucleus. Reconstructed with 2,000 frames (17.7 ms/frame). **d**, Nucleosomal arrays. **e**,

Chromatin fibers. FWHM (x, y, z) in nm (from top to bottom): 30, 30, 107; 35, 42, 124; 34, 51, 102; 69, 51, 154. Localization precision (nm): 7.6, 6.8, 6.8, 9.5. **f**, 3D sizes of chromatin fibers by FWHM. N = 396 from 4 cells, identified in 500 frames. **g**, Distribution of chromatin fibers (identified in 500 frames). **h**, Fast dynamics of a chromatin fiber. Snapshots from Supplementary Videos 7 and 8 (Supplementary Information, video legends). Scale bar: 5 μm in **b**; **c** and **g**; 200 nm in **d**, **e** and **h**. Laser intensity: 3.2 kW/cm^2 at 656 nm. Axial position (nm) represented by RGB color depth coding.

A previous cryo-electron tomography (cryo-ET) study identified short chromatin fibers with 30 nm in diameter in isolated nuclei from chicken erythrocytes[31]. Therefore, we also attempted 3D SMLM experiments on living chicken erythrocytes with **6-HoeHESiR**. By applying a modest laser intensity of 950 W/cm^2, 3D chromatin structures in chicken erythrocyte nuclei were successfully visualized (Fig. 5a-c; Supplementary Fig. 12a; Supplementary Video 16). The same two categories of chromatin structures were observed, and chromatin fibers were identified with a mean localization precision of 8 nm, average 3D size (FWHM) of 32, 35, 90 nm (x, y, z) and a higher labeling density of 56,494 molecules/μm^3 (Fig. 5d-g; Supplementary Fig. 12b-d; Supplementary Videos 17 and 18). The fast dynamics of chromatin structures in chicken erythrocyte nuclei were also observed (Supplementary Video 19), with the mean resting lifetime of chromatin fibers estimated to be 1 second.

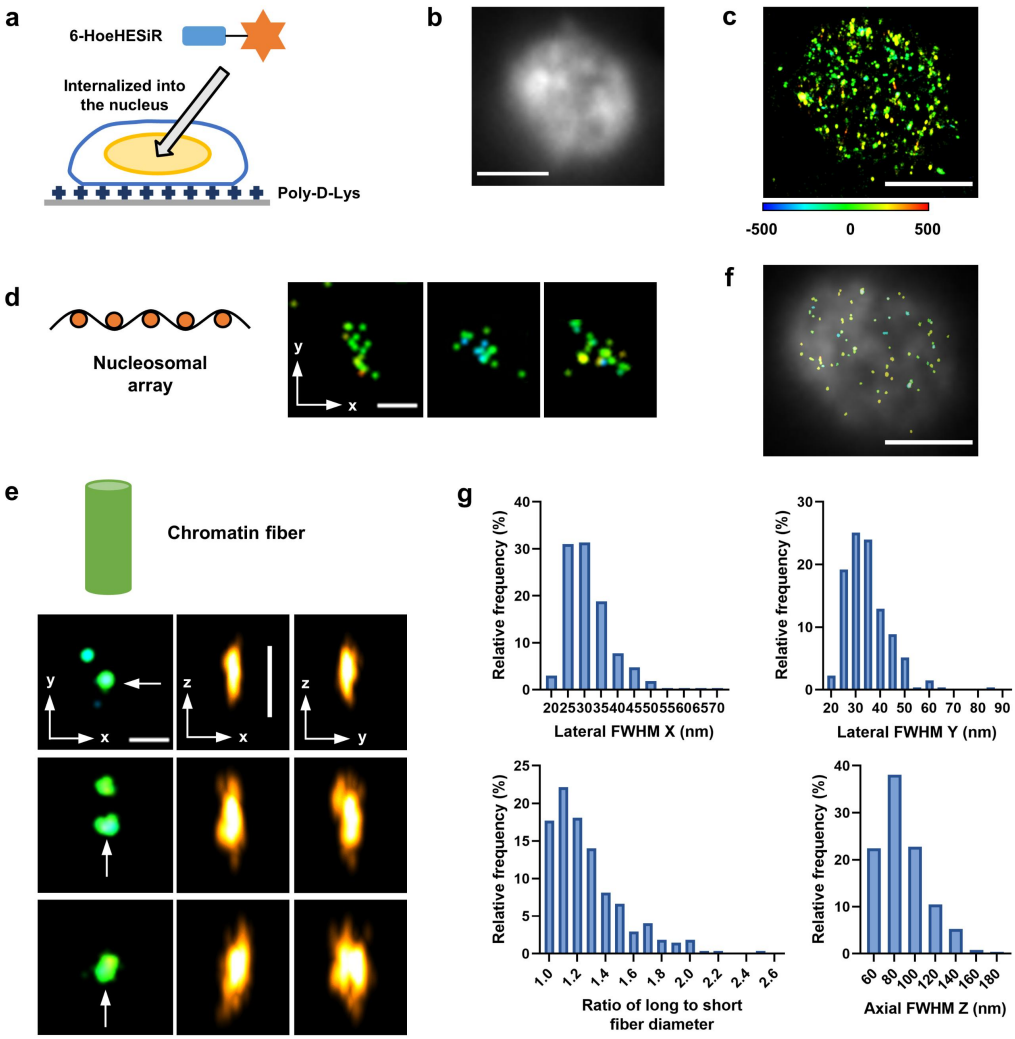

Fig. 5 Native chromatin 3D structures in living chicken erythrocytes. a, Schematic illustration of chromatin labeling with **6-HoeHESiR** (0.5 μM for 10 min). **b,** Image of a nucleus by widefield microscopy. **c**, Image of a nucleus. Reconstructed with 10,000 frames (17.7 ms/frame). **d**, Nucleosomal arrays. **e**, Chromatin fibers. FWHM (x, y, z) in nm (from top to bottom): 27, 29, 83; 37, 40, 124; 40, 62, 95. Localization precision (nm): 6.8, 6.9, 8.1. **f**, 3D sizes of chromatin fibers by FWHM. $N = 268$ from 3 cells, identified in 5,000 frames. **g**, Distribution of chromatin fibers (identified in 5,000 frames). Scale bar: 2 μm in **b**, **c** and **g**; 200 nm in **d** and **e**. Laser intensity: 0.95 kW/cm^2 at 656 nm. Axial position (nm) represented by RGB color depth coding.

The connection between 3D chromatin organization and histone acetylation

251 It is known that histone acetylation is a critical epigenetic marker for chromatin fiber relaxation and
252 optimal transcription, whereas histone deacetylation is required for chromatin fiber condensation and
253 transcriptional repression[32]. Inhibition of histone deacetylases (HDACs), key enzymes that reduce
254 histone acetylation, is an important approach to anticancer drug development by inducing chromatin
255 decompaction and reactivating tumor suppressor genes[33,34]. To investigate the connection between
256 chromatin fibers and histone acetylation status in living cells, we selected three HDAC inhibitors (Fig.
257 6a): 1) trichostatin A (TSA), a widely used HDAC pan-inhibitor; 2) entinostat, a class I HDAC 1−3
258 selective inhibitor; and 3) ricolinostat, a class IIb HDAC 6 selective inhibitor. Live HeLa cells were
259 treated with each of these HDAC inhibitors and then imaged by 3D SMLM (Fig. 6b). The image
260 analysis results show that the density of chromatin fibers decreased by 52% and 63% upon treatments
261 with TSA and entinostat, respectively[35,36], whereas no significant change in fiber density was observed
262 upon ricolinostat treatment (Fig. 6c-d, Supplementary Fig. 13-15). These results are consistent with
263 literature reports that the functions of class I HDACs 1−3 are exclusively restricted to the nucleus, while
264 class IIb HDAC 6 functions largely outside the nucleus by mediating the deacetylation of cytosolic
265 proteins[37]. Taken together, our live-cell 3D imaging results provide the first live-cell evidence for the
266 global change in 3D chromatin organization in response to histone hyperacetylation induced by
267 small-molecule HDAC inhibitors.

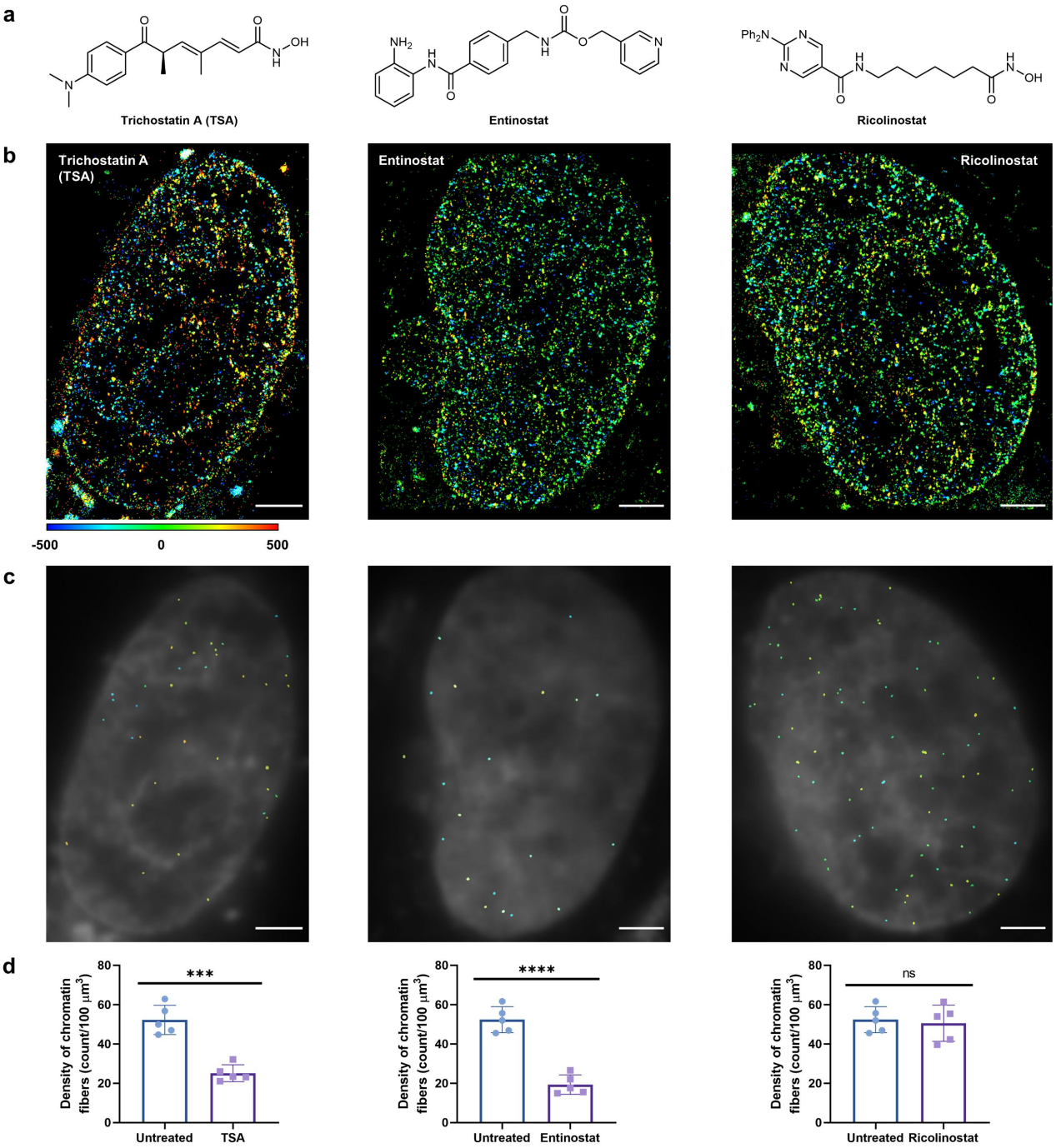

Fig. 6 Decompaction of chromatin fibers induced by HDAC inhibitors. a, Structures of small-molecule inhibitors of HDAC. **b**, Images of the nuclei in treated HeLa cells. Reconstructed with 2,000 frames (17.7 ms/frame). **c**, Distribution of chromatin fibers (identified in 500 frames). **d**, Density of chromatin fibers (identified in 500 frames). Data are individual values and mean ± s.d., N = 5. Statistical significance was determined by *t test* with P = 0.0001, <0.0001 and 0.7278 (from left to right). The scale bar is 2 μm. Laser intensity: 3.2 kW/cm^2 at 656 nm. Axial position (nm) represented by RGB

275 color depth coding. Cells were treated with TSA (200 nM), entinostat (2 μM), and ricolinostat (1 μM)
276 for 20 h, respectively, and then incubated with **6-HoeHESiR** (5 μM) for 30 min.

277 **DISCUSSION**

278 To summarize, we have demonstrated the success of developing a self-blinking Si-rhodamine dye
279 **6-HESiR** and a self-blinking fluorogenic DNA probe **6-HoeHESiR** by structurally fine-tuning the "ON"
280 state population to a suitable level. This design strategy has proven effective in 3D imaging of *in vitro*
281 reconstituted chromatin samples and native chromatin in both fixed cells and living cells by SMLM. It
282 is noteworthy that high spatiotemporal resolution and labeling density were achieved in live-cell 3D
283 SMLM even at a reduced laser intensity that alleviates phototoxicity. Consequently, we were able to
284 observe native chromatin organized in hierarchical forms of nucleosomal arrays and chromatin fibers
285 with fast dynamics and structural polymorphism. Our imaging results are consistent with recent
286 RICC-seq[27] and high-resolution Micro-C[28] studies that support the existence of chromatin fibers in
287 mammalian cells and budding yeasts. To the best of our knowledge, we have obtained the first live-cell
288 evidence for a hierarchical model of chromatin organization[38-40] (Fig. 7), through which the 2-m long
289 genomic DNA is highly compacted and packaged into the 10-μm eukaryotic nucleus. The structural
290 plasticity/heterogeneity and fast dynamics of chromatin fibers are consistent with the complex
291 regulatory environment in the nucleus, such as histone modifications and variants, nonhistone
292 architectural proteins, and linker DNA lengths for various biological functions[38-40]. The
293 density/population of chromatin fibers was reduced by small-molecule inhibitors of HDACs that are
294 responsible for histone deacetylation. For the first time, this phenomenon provides a live-cell 3D view
295 of the tight connection between the histone acetylation state and chromatin hierarchical organization
296 with unprecedented resolution. In light of our initial success, we anticipate further in-depth studies on
297 the structures and functions of chromatin fibers in DNA-related processes in living cells. We also
298 envision that our structural fine-tuning strategy could be implemented to develop more self-blinking

fluorophores and probes to enable the study of subcellular organelles and biological events by live-cell 3D superresolution imaging.

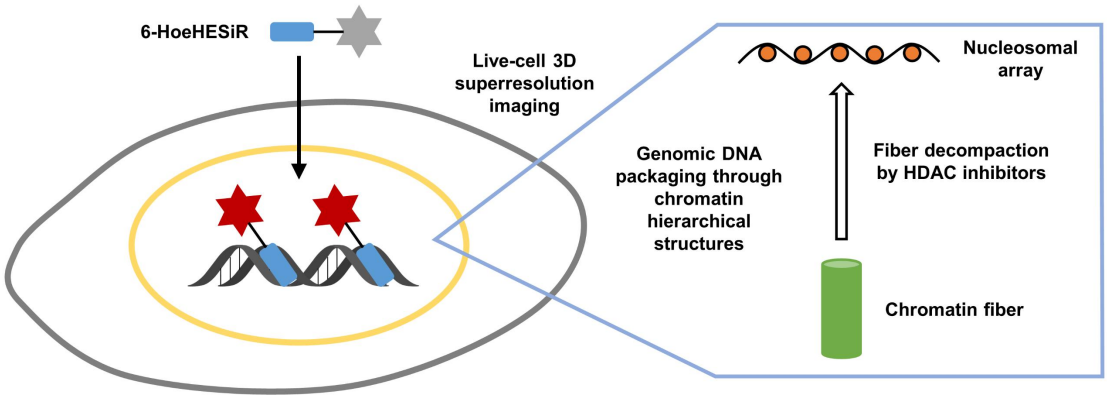

Fig. 7 Schematic illustration of genomic DNA packaging via hierarchical chromatin structures.

Acknowledgments

We thank the HKU Li Ka Shing Faculty of Medicine Imaging and the Flow Cytometry Core of CPOS for support in cell imaging. This work was supported by The University of Hong Kong, Westlake University, Morningside Foundation, and Hong Kong Research Grants Council under the Area of Excellence Scheme (AoE/P-705/16 to D.Y.). This work was supported by grants for G.L. from the National Natural Science Foundation of China (31991161), the Ministry of Science and Technology of China (2017YFA0504202), the Beijing Municipal Science and Technology Commission (Z201100005320013) and the HHMI International Research Scholars Program (55008737). R. L. was supported by the ECS (grant number 27204518) of the Hong Kong SAR government and by the URC fund at the University of Hong Kong. We thank Dr. Teng Zhao and Dr. Zhe Hu for their technical support in light-sheet microscopy. We thank Dr. Zhe Hu, Dr. Teng Zhao, Dr. Shengwang Du and Dr. Wei Li for helpful discussions. We thank Dr. Nai-Kei Wong and Ms. Jasmine Chit Ying Lau for proofreading the manuscript.

Author contributions

Y.Z. and G.L. conceived the idea. G.L. and D.Y. supervised the project. Y.Z. designed **6-HESiR** and **6-HoeHESiR**. Y.Z. performed chemical synthesis and characterization with contribution from R.X. Y.Z. studied photophysical properties with contribution from S.Y. C.L. prepared *in vitro* reconstituted samples and performed electron microscopy analysis. S.-H.L. performed the SMLM experiment with lambda DNA and analyzed the data. Y.Z., S.Y. and S.D. performed cell culture and treatment. Z.Z. performed budding yeast culture. Y.Z. and S.Y. performed SMLM experiments with reconstituted chromatin structures and with fixed and live cells. Y.C. and Y.L. performed the SMLM validation experiments. L.H. performed cytotoxicity assay. S.-M.L. developed the computer program and the web server for chromatin fiber analysis under the supervision of R.L. Y.Z. analyzed chromatin imaging data and performed statistical analysis with contribution from S.Y. and S.-M.L. Y.Z., S.Y., G.L. and D.Y. interpreted imaging results with contribution from all other authors. Y.Z., S.Y., G.L. and D.Y. wrote the manuscript with input from all other authors.

Competing interests

The authors declare no competing interests.

Data availability

All data that support the findings of this manuscript are provided in text, figures, and supplementary videos. Original data are provided upon reasonable request to the correspondence authors.

REFERENCES

1. Liu, Z., Lavis, Luke D. & Betzig, E. Imaging Live-Cell Dynamics and Structure at the Single-Molecule Level. *Mol. Cell* **58**, 644-659 (2015).
2. Sauer, M. & Heilemann, M. Single-Molecule Localization Microscopy in Eukaryotes. *Chem. Rev.* **117**, 7478-7509 (2017).

339 3. von Diezmann, A., Shechtman, Y. & Moerner, W. E. Three-Dimensional Localization of Single
340 Molecules for Super-Resolution Imaging and Single-Particle Tracking. *Chem. Rev.* **117**,
341 7244-7275 (2017).
342 4. Sahl, S. J., Hell, S. W. & Jakobs, S. Fluorescence nanoscopy in cell biology. *Nat. Rev. Mol. Cell*
343 *Biol.* **18**, 685-701 (2017).
344 5. Sigal, Y. M., Zhou, R. & Zhuang, X. Visualizing and discovering cellular structures with
345 super-resolution microscopy. *Science* **361**, 880-887 (2018).
346 6. Lelek, M. *et al.* Single-molecule localization microscopy. *Nat. Rev. Methods Primers* **1**, 39,
347 (2021).
348 7. Uno, S.-n. *et al.* A spontaneously blinking fluorophore based on intramolecular spirocyclization
349 for live-cell super-resolution imaging. *Nat. Chem.* **6**, 681-689 (2014).
350 8. Tachibana, R. *et al.* Design of spontaneously blinking fluorophores for live-cell super-resolution
351 imaging based on quantum-chemical calculations. *Chem. Commun.* **56**, 13173-13176 (2020).
352 9. Chi, W. *et al.* Descriptor ΔGC-O Enables the Quantitative Design of Spontaneously Blinking
353 Rhodamines for Live-Cell Super-Resolution Imaging. *Angew. Chem. Int. Ed.* **59**, 20215-20223
354 (2020).
355 10. Tyson, J. *et al.* Extremely Bright, Near-IR Emitting Spontaneously Blinking Fluorophores Enable
356 Ratiometric Multicolor Nanoscopy in Live Cells. *ACS Cent Sci* **7**, 1419-1426 (2021).
357 11. Takakura, H. *et al.* Long time-lapse nanoscopy with spontaneously blinking membrane probes. *Nat.*
358 *Biotechnol.* **35**, 773-780 (2017).
359 12. Wäldchen, S., Lehmann, J., Klein, T., van de Linde, S. & Sauer, M. Light-induced cell damage in
360 live-cell super-resolution microscopy. *Sci. Rep.* **5**, 15348 (2015).
361 13. Grimm, J. B. *et al.* A general method to fine-tune fluorophores for live-cell and in vivo imaging.
362 *Nat. Methods* **14**, 987-994 (2017).

363 14. Zheng, Q. *et al.* Rational Design of Fluorogenic and Spontaneously Blinking Labels for
364 Super-Resolution Imaging. *ACS Cent. Sci.* **5**, 1602-1613 (2019).
365 15. Grimm, J. B. *et al.* A general method to optimize and functionalize red-shifted rhodamine dyes.
366 *Nat. Methods* **17**, 815-821 (2020).
367 16. Uno, S.-n., Kamiya, M., Morozumi, A. & Urano, Y. A green-light-emitting, spontaneously
368 blinking fluorophore based on intramolecular spirocyclization for dual-colour super-resolution
369 imaging. *Chem. Commun.* **54**, 102-105 (2018).
370 17. Butkevich, A. N. Modular Synthetic Approach to Silicon-Rhodamine Homologues and Analogues
371 via Bis-aryllanthanum Reagents. *Org. Lett.* **23**, 2604-2609 (2021).
372 18. Nakamura, A. *et al.* Hoechst tagging: a modular strategy to design synthetic fluorescent probes for
373 live-cell nucleus imaging. *Chem. Commun.* **50**, 6149-6152 (2014).
374 19. Lukinavičius, G. *et al.* SiR–Hoechst is a far-red DNA stain for live-cell nanoscopy. *Nat. Commun.*
375 **6**, 8497 (2015).
376 20. Bucevičius, J., Keller-Findeisen, J., Gilat, T., Hell, S. W. & Lukinavičius, G. Rhodamine–Hoechst
377 positional isomers for highly efficient staining of heterochromatin. *Chem. Sci.* **10**, 1962-1970
378 (2019).
379 21. Zhang, X. *et al.* A targetable fluorescent probe for dSTORM super-resolution imaging of live cell
380 nucleus DNA. *Chem. Commun.* **55**, 1951-1954 (2019).
381 22. Bucevičius, J., Kostiuk, G., Gerasimaitė, R., Gilat, T. & Lukinavičius, G. Enhancing the
382 biocompatibility of rhodamine fluorescent probes by a neighbouring group effect. *Chem. Sci.* **11**,
383 7313-7323 (2020).
384 23. Bucevičius, J., Gilat, T. & Lukinavičius, G. Far-red switching DNA probes for live cell nanoscopy.
385 *Chem. Commun.* **56**, 14797-14800 (2020).

386 24. Breusegem, S. Y., Clegg, R. M. & Loontiens, F. G. Base-sequence specificity of Hoechst 33258
387 and DAPI binding to five $(A/T)_4$ DNA sites with kinetic evidence for more than one high-affinity
388 Hoechst 33258-AATT complex. *J. Mol. Biol.* **315**, 1049-1061 (2002).
389 25. Zhang, Y. *et al.* Ultrafast, accurate, and robust localization of anisotropic dipoles. *Protein & Cell* **4**,
390 598-606 (2013).
391 26. Li, W. *et al.* FACT Remodels the Tetranucleosomal Unit of Chromatin Fibers for Gene
392 Transcription. *Mol. Cell* **64**, 120-133 (2016).
393 27. Risca, V. I., Denny, S. K., Straight, A. F. & Greenleaf, W. J. Variable chromatin structure revealed
394 by in situ spatially correlated DNA cleavage mapping. *Nature* **541**, 237-241 (2017).
395 28. Hsieh, T.-H. S. *et al.* Resolving the 3D Landscape of Transcription-Linked Mammalian Chromatin
396 Folding. *Molecular Cell* **78**, 539-553.e538 (2020).
397 29. Ricci, Maria A., Manzo, C., García-Parajo, M. F., Lakadamyali, M. & Cosma, Maria P. Chromatin
398 Fibers Are Formed by Heterogeneous Groups of Nucleosomes In Vivo. *Cell* **160**, 1145-1158
399 (2015).
400 30. Nozaki, T. *et al.* Dynamic Organization of Chromatin Domains Revealed by Super-Resolution
401 Live-Cell Imaging. *Mol. Cell* **67**, 282-293 (2017).
402 31. Scheffer, M. P., Eltsov, M. & Frangakis, A. S. Evidence for short-range helical order in the 30-nm
403 chromatin fibers of erythrocyte nuclei. *Proc. Natl. Acad. Sci. U.S.A.* **108**, 16992-16997 (2011).
404 32. Li, G. *et al.* Highly Compacted Chromatin Formed In Vitro Reflects the Dynamics of
405 Transcription Activation In Vivo. *Mol. Cell* **38**, 41-53 (2010).
406 33. Li, Y. & Seto, E. HDACs and HDAC Inhibitors in Cancer Development and Therapy. *Cold Spring*
407 *Harb. Perspect. Med.* **6**, a026831 (2016).
408 34. Eckschlager, T., Plch, J., Stiborova, M. & Hrabeta, J. Histone Deacetylase Inhibitors as Anticancer
409 Drugs. *Int. J. Mol. Sci.* **18**, 1414 (2017).

410 35. Tóth, K. F. *et al.* Trichostatin A-induced histone acetylation causes decondensation of interphase
411 chromatin. *J. Cell Sci.* **117**, 4277-4287 (2004).
412 36. Otterstrom, J. *et al.* Super-resolution microscopy reveals how histone tail acetylation affects DNA
413 compaction within nucleosomes in vivo. *Nucleic Acids Res.* **47**, 8470-8484 (2019).
414 37. Fallah, M. S., Szarics, D., Robson, C. M. & Eubanks, J. H. Impaired Regulation of Histone
415 Methylation and Acetylation Underlies Specific Neurodevelopmental Disorders. *Front. Genet.* **11**,
416 613098 (2021).
417 38. Li, G. & Reinberg, D. Chromatin higher-order structures and gene regulation. *Curr. Opin. Genet.*
418 *Dev.* **21**, 175-186 (2011).
419 39. Luger, K., Dechassa, M. L. & Tremethick, D. J. New insights into nucleosome and chromatin
420 structure: an ordered state or a disordered affair? *Nat. Rev. Mol. Cell Biol.* **13**, 436-447 (2012).
421 40. Chen, P., Li, W. & Li, G. Structures and Functions of Chromatin Fibers. *Annu. Rev. Biophys.* **50**,
422 95-116 (2021).